ISSN 1936-878X/09/$36.00
PUBLISHED BY ELSEVIER INC.
DOI:10.1016/j.jcmg.2009.04.016

^{18}F-4V for PET–CT Imaging of VCAM-1 Expression in Atherosclerosis

Matthias Nahrendorf, MD, PhD,*†‡ Edmund Keliher, PhD,*† Peter Panizzi, PhD,† Hanwen Zhang, PhD,† Sheena Hembrador, BS,† Jose-Luiz Figueiredo, MD,*† Elena Aikawa, MD,† Kimberly Kelly, PhD,† Peter Libby, MD,‡§ Ralph Weissleder, MD, PhD*†‡

Boston and Charlestown, Massachusetts

OBJECTIVES The aim of this study was to iteratively develop and validate an ^{18}F-labeled small vascular cell adhesion molecule (VCAM)-1 affinity ligand and demonstrate the feasibility of imaging VCAM-1 expression by positron emission tomography–computed tomography (PET-CT) in murine atherosclerotic arteries.

BACKGROUND Hybrid PET-CT imaging allows simultaneous assessment of atherosclerotic lesion morphology (CT) and may facilitate early risk assessment in individual patients. The early induction, confinement of expression to atherosclerotic lesions, and accessible position in proximity to the blood pool render the adhesion molecule VCAM-1 an attractive imaging biomarker for inflamed atheroma prone to complication.

METHODS A cyclic, a linear, and an oligomer affinity peptide, internalized into endothelial cells by VCAM-1–mediated binding, were initially derivatized with DOTA to determine their binding profiles and pharmacokinetics. The lead compound was then ^{18}F-labeled and tested in atherosclerotic apoE$^{-/-}$ mice receiving a high-cholesterol diet as well as wild type murine models of myocardial infarction and heart transplant rejection.

RESULTS The tetrameric peptide had the highest affinity and specificity for VCAM-1 (97% inhibition with soluble VCAM-1 in vitro). In vivo PET-CT imaging using ^{18}F-4V showed 0.31 $\pm$ 0.02 SUV in murine atheroma (ex vivo %ID/GT 5.9 $\pm$ 1.5). ^{18}F-4V uptake colocalized with atherosclerotic plaques on Oil Red O staining and correlated to mRNA levels of VCAM-1 measured by quantitative reverse transcription polymerase chain reaction ($R = 0.79$, $p = 0.03$). Atherosclerotic mice receiving an atorvastatin-enriched diet had significantly lower lesional uptake ($p < 0.05$). Furthermore, ^{18}F-4V imaging in myocardial ischemia after coronary ligation and in transplanted cardiac allografts undergoing rejection showed high in vivo PET signal in inflamed myocardium and good correlation with ex vivo measurement of VCAM-1 mRNA by quantitative polymerase chain reaction.

CONCLUSIONS ^{18}F-4V allows noninvasive PET-CT imaging of VCAM-1 in inflammatory atherosclerosis, has the dynamic range to quantify treatment effects, and correlates with inflammatory gene expression. (J Am Coll Cardiol Img 2009;2:1213–22) © 2009 by the American College of Cardiology Foundation

From the *Center for Systems Biology, Massachusetts General Hospital and Harvard Medical School, Boston, Massachusetts; †Center for Molecular Imaging Research, Massachusetts General Hospital and Harvard Medical School, Charlestown, Massachusetts; ‡Donald W. Reynolds Cardiovascular Clinical Research Center on Atherosclerosis at Harvard Medical School, Boston, Massachusetts; and the §Cardiovascular Division, Department of Medicine, Brigham & Women's Hospital, Boston, Massachusetts. This work was funded in part by the D.W. Reynolds Foundation (to Drs. Libby and Weissleder), UO1-HL080731 (to Dr. Weissleder), R01-HL078641 (to Dr. Weissleder), and R24-CA92782 (to Dr. Weissleder). Drs. Keliher, Panizzi, and Zhang contributed equally to this article.

Manuscript received March 2, 2009; revised manuscript received March 31, 2009, accepted April 23, 2009.

JACC: CARDIOVASCULAR IMAGING, VOL. 2, NO. 10, 2009
OCTOBER 2009:1213–22

A reliable noninvasive diagnostic strategy for detecting inflamed arterial lesions at risk for complications could help target and evaluate therapies to prevent myocardial infarction (MI) and stroke. Current clinical imaging technologies largely provide structural information (1); however, the anatomical severity of stenosis does not sufficiently gauge the risk of vascular events (2). Molecular imaging approaches now in development aim to interrogate biological processes rather than morphology (1,3,4).

ABBREVIATIONS AND ACRONYMS

^{18}F-4V = ^{18}F-labeled tetrameric peptide-PET imaging reporter targeted to VCAM-1

^{18}FDG = [^{18}F]-fluorodeoxyglucose

ApoE = apolipoprotein E

DOTA = 1,4,7,10-tetraazadodecane-1,4,7,10-tetraacetic acid, chelator for 111-Indium labeling

MCP = monomeric cyclic peptide (DOTA-labeled)

MHEC = murine heart endothelial cells

MLP = monomeric linear peptide (DOTA-labeled)

MI = myocardial infarction

mRNA = messenger ribonucleic acid

%IDGT = percent injected dose/gram tissue

PET-CT = positron emission tomography-computed tomography

RT-PCR = reverse transcription polymerase chain reaction

TLP = tetrameric linear peptide (DOTA-labeled)

VCAM = vascular cell adhesion molecule

See page 1223

Vascular cell adhesion molecule (VCAM)-1 plays a cardinal role in atherosclerotic plaque progression (5–7). Activated endothelial cells that line the tissue-blood interface express VCAM-1, as can lesional macrophages and smooth muscle cells (5–7). VCAM-1 mediates inflammatory cell adhesion through interaction with the integrin very late antigen-4 (8). The early induction, confinement of expression to atherosclerotic lesions, and accessible position in proximity to the blood pool render VCAM-1 an attractive imaging biomarker.

We (9,10) and others (11,12) have imaged VCAM-1 as a proof-of-principle in inflammatory disease, for instance with targeted nanoparticles for magnetic resonance imaging (MRI). Although providing early efficacy data, these agents face practical regulatory hurdles that prevent rapid clinical development. Despite the specific advantages of positron emission tomography (PET), the increasing clinical availability of PET-computed tomography (CT) scanners, and the unmet need for noninvasive identification of high-risk vascular lesions, relatively few targeted PET agents exist for plaque imaging (13,14). [^{18}F]-2-fluorodeoxyglucose (^{18}FDG) can accumulate in atherosclerotic lesions (15–17) and is clinically approved for cancer imaging. ^{18}FDG uptake presumably indicates glucose transport, and uptake associates with macrophage (18) and neovessel content (19). Studies in patients undergoing endarterectomy (17) showed increased ^{18}FDG signal in macrophage-rich carotid arteries. However, there remains a need for development of agents that selectively target inflammation in plaques and that have lower background uptake in metabolically highly active myocardial tissue than ^{18}FDG to facilitate coronary imaging.

Here we describe the design, synthesis, evaluation, and use of a new PET imaging agent with optimized pharmacokinetics and specificity for VCAM-1. The overall design of this peptide-based agent hinged on: 1) preference of PET-CT as a hybrid clinical imaging modality with high-sensitivity (PET) combined with detailed anatomical information (CT); 2) choice of ^{18}F as a clinical PET tracer with a short half-life; 3) harnessing powerful signal amplification strategies (multivalency of affinity ligand and VCAM-1–mediated cell internalization); and 4) choice of a probe design that would ultimately allow for rapid clinical translation.

METHODS

Agent synthesis. A number of VCAM-1 specific peptide sequences have been identified by phage display technology (9,10) containing linear and cyclic heptapeptides (Table 1). To facilitate comparative testing of agents in the current work, we first derivatized 3 lead peptides with the chelator 1,4,7,10-tetraazadodecane-1,4,7,10-tetraacetic acid (DOTA) and labeled them with ^{111}Indium. Peptides were synthesized with standard Nα-9-fluorenylmethoxycarbonyl chemistry, followed by high-performance liquid chromatographic analysis, which demonstrated >98% purity. The labeling yields of ^{111}In-DOTA derivatives were >99% at specific activities of 30.8 GBq/μmol. On the basis of initial comparative results, we then redesigned the best peptide (sequence VHPKQHR, linker GGSYKKK, tetramer) and labeled it with ^{18}Fluorine with a benzaldehyde method (20). The synthesis of the lead compound, named ^{18}F-4V, was automated with a PETsynthRN synthesizer (Nebeling GmbH, Drolshagen, Germany) followed by high-performance liquid chromatographic purification. We also synthesized a fluorescent version of ^{18}F-4V by conjugating Cy5 maleimide to enable fluorescence microscopy detection of the probe in histological sections.

Competition assays. We evaluated the affinity of peptides in competition assays with murine VCAM-1 immobilized on agarose beads. Tetrameric linear peptide (TLP)-DOTA-^{111}In (37 GBq/μmol, 0.5 nmol/l) was added to VCAM-1/agarose beads, and competed off with increasing concentrations of unlabeled monomeric cyclic peptide (MCP)-DOTA, monomeric linear peptide (MLP)-DOTA, and TLP-DOTA, respectively. After washing, the amount of labeled TLP-DOTA-^{111}In bound to beads was quantitated via gamma well counter. Next, we assessed

Table 1. Summary of Specific VCAM-1 Targeted Peptide Sequences

Name	Peptide Sequence	Linear/Cyclic	Monomer/Tetramer
MCP	CVHSPNKKCGGSYK(DOTA)	Cyclic	Monomer
MLP	VHPKQHRGGSYK(DOTA)	Linear	Monomer
TLP	([VHPKQHRGGSY]2K)2KK(DOTA)	Linear	Tetramer
^{18}F-4V	([VHPKQHRGGSY]2K)2KK(AOE)	Linear	Tetramer

DOTA = 1,4,7,10-tetraazadodecane-1,4,7,10-tetraacetic acid; MCP = monomeric cyclic peptide (DOTA labeled); MLP = monomeric linear peptide (DOTA-labeled); TLP = tetrameric linear peptide (DOTA-labeled); VCAM = vascular cell adhesion molecule; ^{18}F-4V = ^{18}F-labeled tetrameric peptide-PET imaging reporter targeted to VCAM-1.

binding of candidate peptides to VCAM-1–expressing endothelial cells. The ^{111}In-labeled peptides were added to murine heart endothelial cells (MHEC) (21) and incubated at 37°C for 1 h. Cells were harvested from the plates, and the radioactivity was measured via gamma well counter. To evaluate specificity for VCAM-1, ^{18}F-4V (0.20 μg) was preincubated with 5× murine VCAM-1 or saline and then added to MHEC.

Mouse models. Apolipoprotein E (ApoE)$^{-/-}$ mice had an average age of 45 weeks and were on a high-cholesterol diet (Harlan Teklad, Madison, Wisconsin), which produces reliable VCAM-1 expression in atherosclerotic plaques located in the aortic root (10). To test imaging in the setting of therapy, we treated a cohort of apoE$^{-/-}$ mice with atorvastatin (enriched in diet, 0.01% wt/wt) (10). Two additional disease entities known to increase VCAM-1 expression were imaged: MI was induced by coronary ligation (22), and heterotopic allograft heart transplantation from BALB/C into C57/B6 mice was performed (23). Mice were anesthetized for all procedures (isoflurane 2% to 3% v/v, Baxter). The institutional subcommittee on research animal care approved all animal studies.

BIODISTRIBUTION STUDIES. The blood half-life of candidate probes was determined with serial retroorbital bleeds after injection of 150 μCi of a given agent into the tail vein of 6 wild-type mice. After sacrifice (4 h), mice were perfused with 10 ml of saline. Organs were harvested, and their activity was recorded with a gamma counter (1480 Wizard 3-inch, PerkinElmer, Waltham, Massachusetts). Biodistribution data were corrected for decay and residual activity at the injection site. Oil Red O staining depicted the distribution of plaques in apoE$^{-/-}$ aortas, which were subsequently analyzed by digital autoradiography. To evaluate the in vivo specificity of ^{18}F-4V, cohorts of mice were preinjected with an antibody targeted to VCAM-1 (BD Pharmingen, San Diego, California), followed by ^{18}F-4V 60 min later.

FLUORESCENCE AND IMMUNOHISTOLOGY. One hour after injection of Cy5-labeled 125-μg peptide, aortas were harvested for fluorescence microscopy and immunohistochemical detection of VCAM-1 (CD106), endothelial cells (CD31), macrophages (MAC-3) (all BD Pharmingen), and smooth muscle cells (α-actin, Lab Vision, Fremont, California).

PET-CT imaging. PET imaging was initiated 1 h after injection of ^{18}F-4V (325 ± 167 μCi in 200 ± 65 μl) in conjunction with high-resolution vascular CT (Inveon, Siemens, Munich, Germany). The PET data were reconstructed with ordered subsets expectation maximization and filtered back projection algorithms (24), with a spatial resolution approaching approximately 1 mm. For quantitation of PET signal, regions of interest were placed in the aortic root on the basis of anatomical CT imaging. The CT X-ray source was used with a power of 80 kVp and 500 μA, an exposure time of 370 to 400 ms, and an isotropic resolution of 90 μm. During CT acquisition, Isovue-370 (Bracco Diagnostics, Princeton, New Jersey) was infused intravenously.

Quantitative reverse transcription polymerase chain reaction. To validate in vivo PET data, we correlated ^{18}F-4V uptake to expression of VCAM-1 and CD68 quantified by multiplex quantitative polymerase chain reaction (PCR) (TaqMan, Applied Biosystems, Foster City, California) with glyceraldehyde-3-phosphate dehydrogenase as an endogenous control.

Statistics. Results are expressed as mean ± SEM. Unpaired data were compared with the unpaired 2-sided *t* test, and paired data were compared with the paired 2-sided *t* test. The significance level in all tests was 0.05. Due to space limitations of the format, the Methods section has been abbreviated.

RESULTS

In vitro and in vivo screening of candidate peptides. To determine the affinity of candidate compound, we measured displacement of radioactively tagged TLP bound to purified VCAM-1 by cold

MLP, MCP, or TLP. Sigmoidal concentration-dependence curves were observed with an R^2 of 0.984 (TLP), 0.9880 (MLP), and 0.9934 (MCP) (Fig. 1A). The tetrameric, linear peptide formulation TLP had a half-maximal inhibitory concentration for VCAM-1 of 86.6 nmol/l, 232- and 349-fold better than MCP or MLP, respectively.

We then screened candidates against MHEC, which constitutively express high levels of VCAM-1 (21), and observed a significantly higher accumulation of TLP than MLP or MCP (Fig 1B). Finally, candidate peptides injected into apoE$^{-/-}$ mice facilitated evaluation of uptake into atheroma. TLP showed the highest percent injected dose/gram tissue (%IDGT) in excised aortas 60 min after injection (4.8-fold higher than MLP and 2.4-fold higher than MCP), corroborated by highest signal on autoradiography exposure (Figs. 1C and 1D).

Specificity, biodistribution, and half-life of ^{18}F-4V. We next proceeded to synthesize the PET tracer ^{18}F-4V by labeling the lead peptide TLP with ^{18}F via 4-[^{18}F]-fluorobenzaldehyde (Fig. 2). Cell uptake experiments involving inhibition with soluble VCAM-1 resulted in a 97% activity decrease, demonstrating a specificity of ^{18}F-4V (Fig. 3A).

We injected ^{18}F-4V into 6 wild-type mice to established the blood half-life and biodistribution. ^{18}F-4V had a blood half-life of 16 ± 0.6 min (R^2 of fit = 0.96). The biodistribution at 4 h transpired as follows: (%IDGT): kidney, 13.2 ± 2.8; liver, 3.7 ± 1.1; lymph node, 3.7 ± 0.3; spleen, 2.1 ± 0.6; lung, 2.2 ± 0.8; small intestine 1.9 ± 0.4; fat, 1.7 ± 0.1; skin, 1.7 ± 0.6; stomach, 1.7 ± 1.1; esophagus, 1.5 ± 0.5; blood, 1.5 ± 0.4; large intestine, 1.4 ± 0.5; aorta, 1.3 ± 0.4; bone, 1.3 ± 0.4; thymus 0.9 ± 0.3; skeletal muscle, 0.7 ± 0.3; heart, 0.6 ± 0.2; and feces, 0.2 ± 0.1.

^{18}F-4V accumulates in atherosclerotic plaques. We assessed uptake of ^{18}F-4V into atherosclerotic plaques in excised aortas of wild-type mice, apoE$^{-/-}$ mice, and apoE$^{-/-}$ mice treated with atorvastatin. Uptake in the aortic root was 312% higher in apoE$^{-/-}$ mice ($p < 0.05$) (Fig. 3B), when compared with wild type. Autoradiography and en face Oil Red O staining confirmed that activity concentrated in atherosclerotic plaques (Fig. 3C).

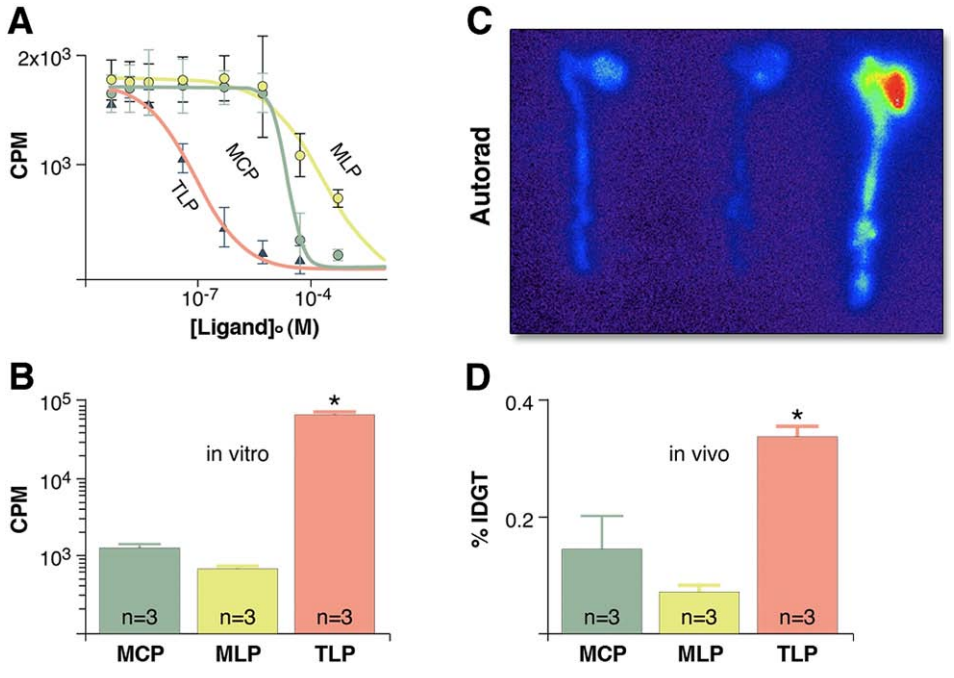

Figure 1. Screening of Affinity Peptides

(A) Affinity curves for ligands assessed by competition after binding to immobilized vascular cell adhesion molecule (VCAM)-1. Tetrameric linear peptide (TLP) has the highest affinity: counts/min (CPM) and mean ± 95% confidence interval. **(B)** Cell assay after incubation of murine heart endothelial cells (MHEC) show highest uptake for TLP. **(C)** Apolipoprotein E (ApoE)$^{-/-}$ mice received injection with ^{111}In-labeled TLP, monomeric cyclic peptide (MCP), and monomeric linear peptide (MLP). Highest autoradiography (Autorad) signal was observed in the root of excised aortas from mice injected with TLP. **(D)** Percent injected dose/gram tissue (%IDGT) in apoE$^{-/-}$ for TLP, MCP, and MLP. Highest %IDGT was observed for TLP. Data are displayed as mean ± SEM, *$p < 0.05$.

Treatment with atorvastatin significantly reduced uptake of ^{18}F-4V (Fig. 3B).

To assess the selectivity of in vivo uptake of ^{18}F-4V for VCAM-1, we pre-injected 250 μg of monoclonal VCAM-1 antibody into apoE$^{-/-}$ mice. This procedure reduced the uptake of the agent to levels seen in wild-type mice (Fig. 3B).

The cellular and microscopic distribution of the agent was assessed with a fluorescently labeled version of the tetrameric peptide and showed good correlation with immunoreactive VCAM-1 expression (Fig. 4). The probe distributed mainly to endothelial and subendothelial layers and colocalized primarily with endothelial cells.

In vivo PET-CT imaging of ^{18}F-4V detects VCAM-1 expression in atherosclerotic plaques. Dynamic PET imaging identified 60 to 120 min after injection as the optimal time period for acquisition (Fig. 5). At that time, we found a strong focal PET signal in the aortic root of apoE$^{-/-}$ mice (Fig. 6). Hybrid imaging facilitated unambiguous allocation of the PET signal to the vascular bed of interest identified by contrast-enhanced vascular CT. Absolute quantification of PET signal (standard uptake value) showed significantly higher values in the root of apoE$^{-/-}$ compared with atorvastatin-treated apoE$^{-/-}$ or wild-type mice (Fig. 6).

Uptake of ^{18}F-4V closely correlates with inflammatory gene expression. After imaging, we determined the ex vivo activity of aortic sections and assessed gene expression by reverse transcription (RT)-PCR (Fig. 7). ^{18}F-4V–derived activity correlated with VCAM-1 mRNA levels ($R = 0.79$, $p = 0.03$) (Fig. 7). We also explored gene expression of CD68, a macrophage biomarker of inflammatory atherosclerosis ($R^2 = 0.50$, $p < 0.05$).

VCAM-1 imaging in other cardiovascular disorders. Given the aforementioned results, we reasoned that ^{18}F-4V PET imaging could apply to a variety of other cardiovascular conditions (e.g., ischemic myocardial injury or transplant rejection), situations that might involve widespread VCAM-1–mediated monocyte recruitment. We assayed VCAM-1 transcript levels in mice 5 days after MI and on day 7 after heart transplantation. The VCAM-1 mRNA levels increased 20- and 3-fold, respectively. As in atherosclerosis, inflamed myocardium had considerable uptake of ^{18}F-4V (Fig. 8). The specificity of this uptake was investigated in vivo with blocking of uptake by preinjection with a VCAM-1 targeted antibody, which reduced the infarct activity/background ratio from 3.1 to 1.4 and, in the transplant model, the graft/background ratio from 2.4 to 1.4.

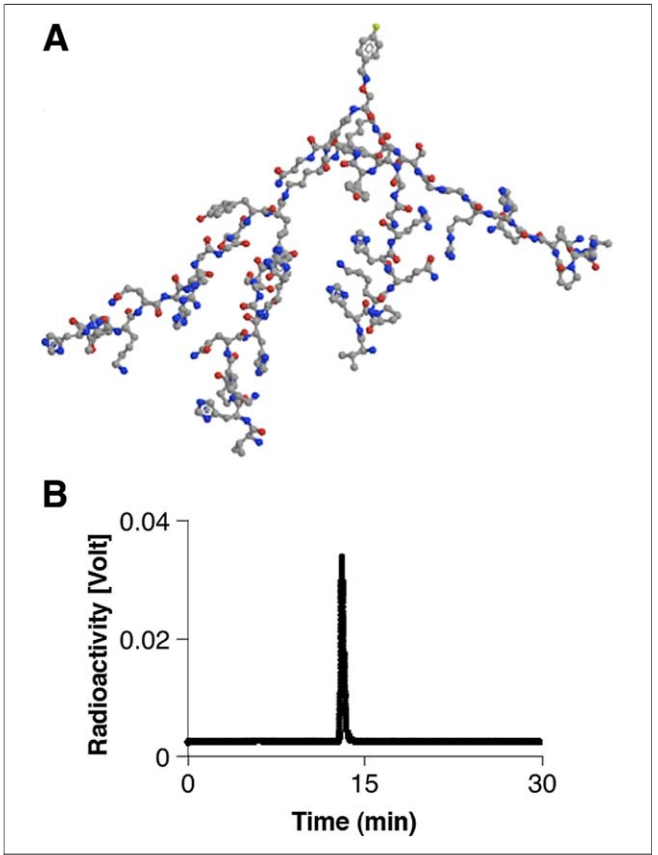

Figure 2. Structure and Purity of ^{18}F-4V

(A) Three-dimensional model of ^{18}F-labeled tetrameric peptide-postitron emission tomography imaging reporter targeted to vascular cell adhesion molecule-1 (^{18}F-4V). The tracer ^{18}F is located on the **top**, and the 4 branching affinity peptides point **downward**. **(B)** Original high-performance liquid chromatographic trace documents purity of the ^{18}F-4V synthesis product.

DISCUSSION

The central role of VCAM-1 in the evolution of inflammatory vascular lesions and its exposed accessible position on the endothelial surface render this adhesion molecule an attractive imaging target for atherosclerosis, MI, and transplant rejection. Here we show that PET-CT can image VCAM-1 and describe the design, synthesis, and validation of the novel PET imaging agent ^{18}F-4V. The technique detects VCAM-1 expression in murine aortas, vessels with a diameter considerably smaller than epicardial human coronary arteries. We also show that targeting VCAM-1 is useful for imaging of other cardiovascular diseases.

The initial design of 3 candidate probes derived from peptides identified by phage display (9,10). Although all of these peptides did target VCAM-1, the modified imaging probes differed in their affin-

JACC: CARDIOVASCULAR IMAGING, VOL. 2, NO. 10, 2009
OCTOBER 2009:1213–22

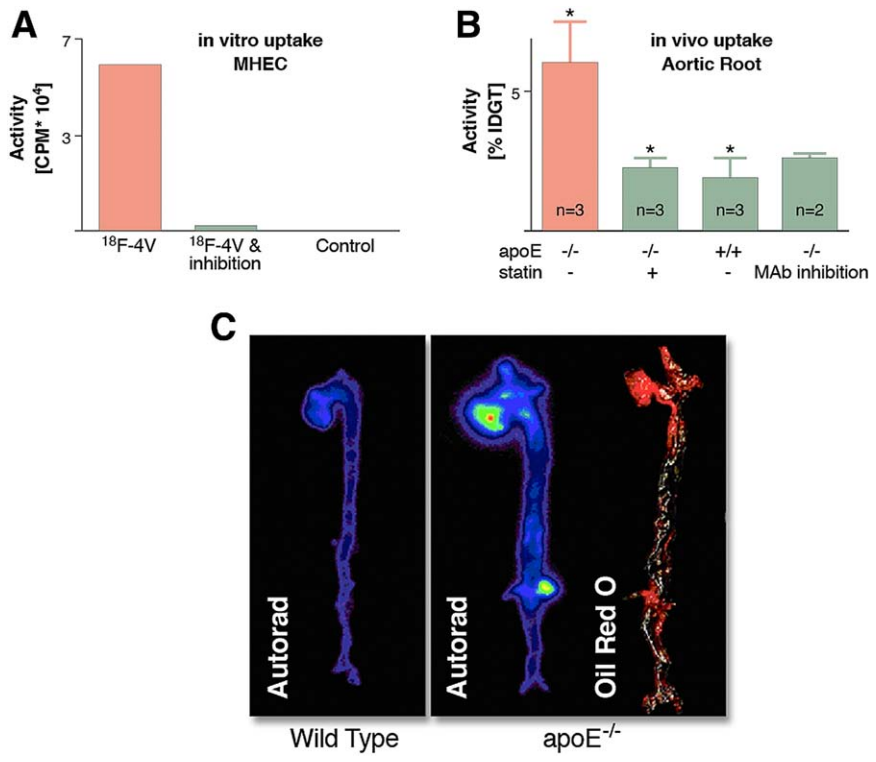

Figure 3. Validation of ^{18}F-4V

(A) Pre-incubation of ^{18}F-4V with soluble VCAM-1 reduces uptake into MHEC. **(B)** Uptake of ^{18}F-4V by scintillation counting. The highest signal was found in aortas of apoE-deficient mice. Statin treatment significantly reduced uptake. Pre-injection of a monoclonal VCAM-1–targeted antibody (MAb) inhibited uptake of ^{18}F-4V. Mean ± SEM, *$p < 0.05$. **(C)** Autoradiography corroborates the highest uptake of ^{18}F-4V in apoE-deficient mice, with little uptake in wild-type aortas. Oil Red O staining shows peak uptake in plaques located in the aortic root, arch, and at the renal artery branch. Abbreviations as in Figures 1 and 2.

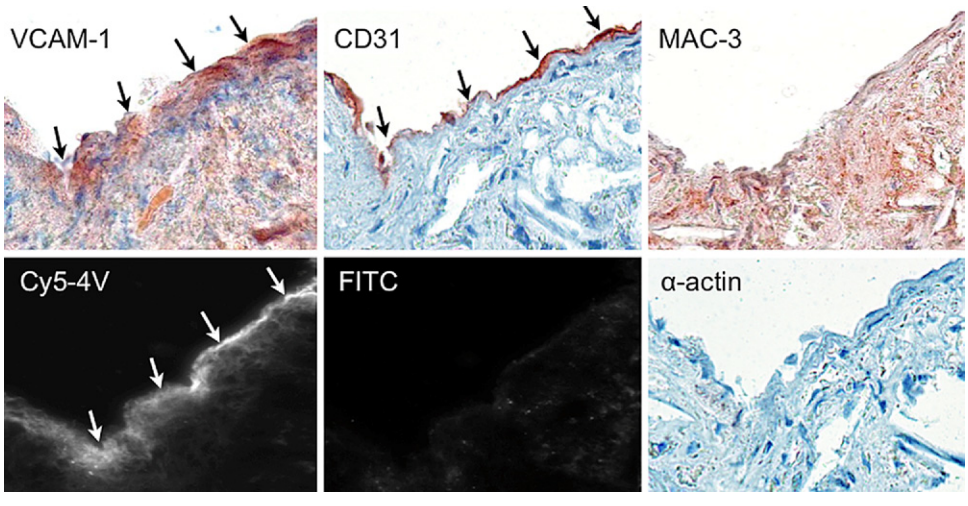

Figure 4. Histologic Probe Distribution

A fluorescent version of ^{18}F-4V (Cy5-4V) was used to explore microscopic and cellular agent distribution. In fluorescence micropscopy, the endothelial and subendothelial layers of an atherosclerotic plaque in the aortic root show strong uptake, whereas autofluorescence in the FITC channel is negligible. On adjacent sections, VCAM-1 and endothelial staining (CD31) colocalize with the agent, with some uptake in macrophages (MAC-3) and smooth muscle cells (α-actin). Magnification 400×.

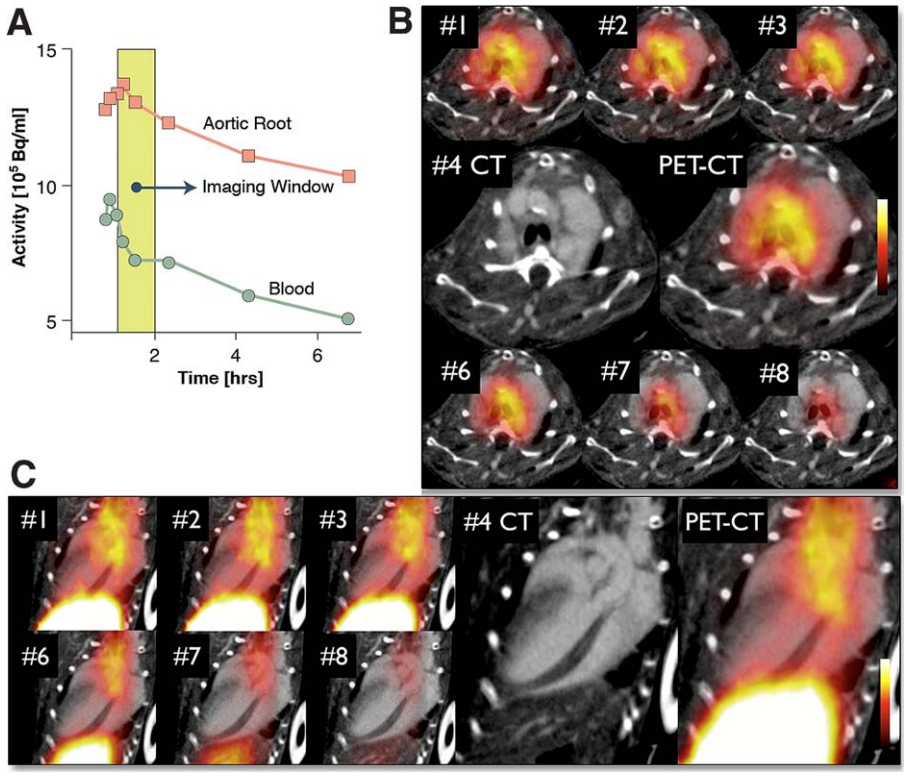

Figure 5. Dynamic PET-CT Imaging

Dynamic positron emission tomography (PET) imaging identified 60 to 120 min after injection as a suitable time window, with low blood signal and high activity in the target. The blood activity was measured in the left ventricular blood pool. Imaging signal in the blood pool and the aortic region is plotted **(A)** and shown over time in short- **(B)** and long-axis **(C)** PET–computed tomography (CT) acquisitions. Initially, acquisition times were shorter due to high count rates, whereas progressing decay of ^{18}F necessitated longer acquisition times in later acquisitions.

ity, molecular weight, and pharmacokinetics. TLP, the lead peptide with the highest affinity and most favorable pharmacokinetics, had an arborizing, tetrameric design. The multivalency of TLP resulted in superior performance, a phenomenon previously observed for targeted nanoparticles (25). Consequently, we derivatized TLP with the clinical PET tracer ^{18}F and investigated ^{18}F-4V in a number of in vitro and in vivo experiments. In vitro, preincubation of the agent with soluble VCAM-1 almost completely blocked cellular uptake. In vivo, pre-injection of a VCAM-1–specific antibody blocked ^{18}F-4V uptake, and ^{18}F-4V signal correlated closely with VCAM-1 mRNA levels in respective vascular territories ($R = 0.79$). Areas of highest activity colocalized with Oil Red O–stained atherosclerotic plaques on excised aortas. Statin treatment, known to reduce VCAM-1 expression (26), diminished the ex vivo and in vivo ^{18}F-4V signal. The biodistribution of ^{18}F-4V proved favorable, with low background uptake in undiseased vessel walls and a short blood half-life, which will allow for rapid injection-imaging sequences.

VCAM-1 expression contributes to the pathophysiology of a variety of other cardiovascular conditions—for instance to inflammation after ischemic injury (11,22,27). Myocardial infarction triggers a profound influx of neutrophils and monocytes on days 1 to 6 after ischemia, and the quantity as well as quality of the myeloid cell influx determine the degree of ensuing heart failure and therefore prognosis (27–29). As an integral part of the recruiting mechanism for monocytes, VCAM-1 expression could gauge the degree of inflammation after MI. We found a substantial increase of VCAM-1 mRNA levels in mice on day 5 after coronary ligation, consistent with ^{18}F-4V accumulation.

VCAM-1 also rises during cardiac transplant rejection and promotes monocyte recruitment into the graft (30,31). Mononuclear phagocytes constitute up to 60% of the inflammatory cell population during parenchymal rejection (32). Patients after heart trans-

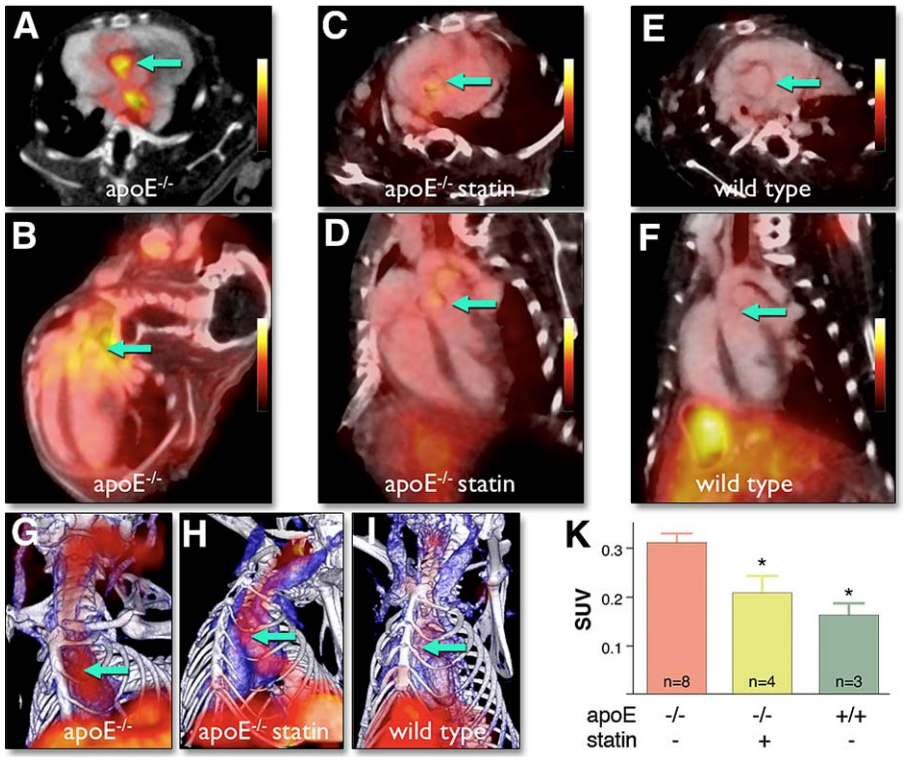

Figure 6. PET-CT in ApoE$^{-/-}$ and Statin-Treated Mice

PET-CT imaging shows uptake of ^{18}F-4V in the aortic root **(arrows)** and arch of atherosclerotic mice. Uptake is lower in statin-treated and in wild-type mice. **(A, C, E)** Short-axis views. **(B, D, F)** Long-axis views. **(G, H, I)** Three-dimensional maximum intensity projection. Bone is shown in white, vasculature in blue, and ^{18}F-4V PET signal in red. The PET signal occurs in the carotid arteries, and background signal in the liver, in addition to the strong uptake of ^{18}F-4V PET observed in the root and arch **(arrow)**. K = quantification of PET signal as the standard uptake value (SUV). Mean ± SEM, *p < 0.05. Abbreviations as in Figures 1, 2, and 5.

plantation would greatly benefit from noninvasive assessment of rejection, because repetitive endomyocardial biopsies, the current reference standard, involve invasion and carry a risk of complication. VCAM-1 mRNA levels increased in heterotopically transplanted cardiac allografts, and the ^{18}F-4V signal indeed rose in these rejecting allografts.

Compared with previous efforts to visualize VCAM-1 by MRI or ultrasound (9,10,12,33), ^{18}F-4V imaging provides a number of potential advantages. Positron emission tomography affords absolute signal quantification and will allow robust and noninvasive measurement of VCAM-1 expression, critical for assessment of individual patients as well as patient cohorts in clinical trials. Not only do high affinity and specificity for a target essential to lesion biology support the translatability of ^{18}F-4V, so too does its employment of a clinically established PET tracer and its clinically useful probe design. The inherent sensitivity of PET allows detection of targets at concentrations that are several orders of magnitude lower than are seen with other modalities, for instance MRI. This feature might have particular importance when targets are as small as atherosclerotic plaques.

Acknowledgments

The authors acknowledge the help of Peter Waterman, BS, Gregory Wojtkiewicz, MS, Brett Martinelli, BS, Yoshiko Iwamoto, BS, and Timur Shtatland, PhD.

Reprint requests and correspondence: Dr. Ralph Weissleder, Massachusetts General Hospital, Center for Systems Biology, CPZN-5206, 185 Cambridge Street, Boston, Massachusetts 02124. *E-mail: rweissleder@mgh.harvard.edu.*

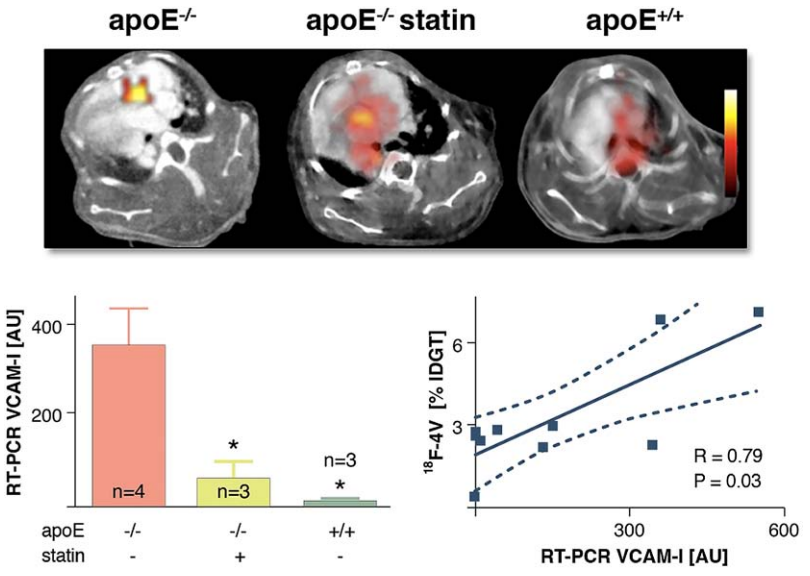

Figure 7. Correlation of ^{18}F-4V Uptake With VCAM-1 Gene Expression

Correlation of ^{18}F-4V uptake to VCAM-1 mRNA levels in imaged vascular segments. After measuring uptake by scintillation counting, gene expression was determined by quantitative RT PCR. When compared with VCAM-1 expression in the root of high-cholesterol–fed apoE-deficient mice, atorvastatin significantly reduced expression, which was very low in wild-type mice. VCAM-1 mRNA levels were normalized to the glyceraldehyde-3-phosphate dehydrogenase housekeeping gene. Data are displayed as mean ± SEM, *$p < 0.05$. The **lower panel** depicts a close correlation of VCAM-1 mRNA level with uptake of ^{18}F-4V. AU = arbitrary units; other abbreviations as in Figures 1 and 2.

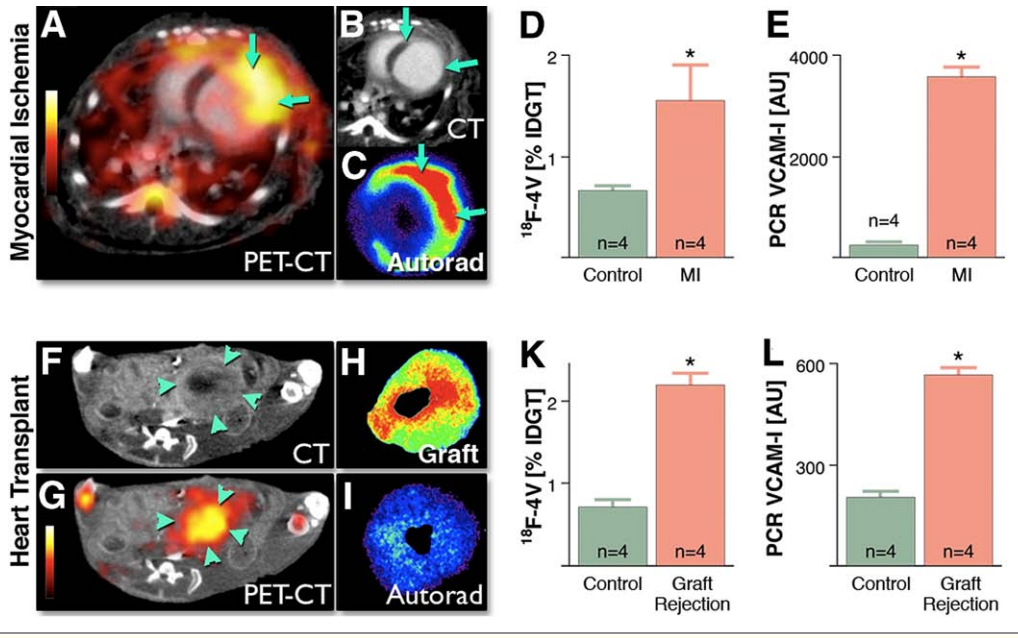

Figure 8. ^{18}F-4V Imaging in MI and Transplant Rejection

(A) PET-CT shows strong signal in the infarcted left ventricular wall. **(B)** Infarcted myocardium shows delayed CT hyperenhancement after iodine **(arrows)**. **(C)** Autoradiography of myocardial ring. **(D)** %IDGT in the infarct. **(E)** VCAM-1 mRNA in infarct tissue. **(F, G)** PET-CT of a heart transplanted heterotopically into the abdominal cavity. The rejected allograft **(arrowheads)** shows high uptake of ^{18}F-4V. **(H, I)** Autoradiography of graft and orthotopic recipient heart. **(K)** Uptake of ^{18}F-4V in rejected allografts. **(L)** VCAM-1 mRNA levels in control heart tissue and rejected cardiac allografts. *$p < 0.05$. MI = myocardial infarction; other abbreviations as in Figures 1, 2, 5, and 7.

REFERENCES

1. Sanz J, Fayad ZA. Imaging of atherosclerotic cardiovascular disease. Nature 2008;451:953–7.
2. Falk E, Shah PK, Fuster V. Coronary plaque disruption. Circulation 1995; 92:657–71.
3. Cyrus T, Lanza GM, Wickline SA. Molecular imaging by cardiovascular MR. J Cardiovasc Magn Reson 2007; 9:827–43.
4. Jaffer FA, Libby P, Weissleder R. Molecular imaging of cardiovascular disease. Circulation 2007;116:1052–61.
5. Iiyama K, Hajra L, Iiyama M, et al. Patterns of vascular cell adhesion molecule-1 and intercellular adhesion molecule-1 expression in rabbit and mouse atherosclerotic lesions and at sites predisposed to lesion formation. Circ Res 1999;85:199–207.
6. Li H, Cybulsky MI, Gimbrone MA Jr., Libby P. Inducible expression of vascular cell adhesion molecule-1 by vascular smooth muscle cells in vitro and within rabbit atheroma. Am J Pathol 1993;143:1551–9.
7. Libby P, Li H. Vascular cell adhesion molecule-1 and smooth muscle cell activation during atherogenesis. J Clin Invest 1993;92:538–9.
8. Libby P. Inflammation in atherosclerosis. Nature 2002;420:868–74.
9. Kelly KA, Allport JR, Tsourkas A, Shinde-Patil VR, Josephson L, Weissleder R. Detection of vascular adhesion molecule-1 expression using a novel multimodal nanoparticle. Circ Res 2005;96:327–36.
10. Nahrendorf M, Jaffer FA, Kelly KA, et al. Noninvasive vascular cell adhesion molecule-1 imaging identifies inflammatory activation of cells in atherosclerosis. Circulation 2006;114:1504–11.
11. Behm CZ, Kaufmann BA, Carr C, Lankford M, Sanders JM, Rose CE, Kaul S, Lindner JR. Molecular imaging of endothelial vascular cell adhesion molecule-1 expression and inflammatory cell recruitment during vasculogenesis and ischemia-mediated arteriogenesis. Circulation 2008;117: 2902–11.
12. McAteer MA, Sibson NR, von Zur Muhlen C, et al. In vivo magnetic resonance imaging of acute brain inflammation using microparticles of iron oxide. Nat Med 2007;13:1253–8.
13. Elmaleh DR, Fischman AJ, Tawakol A, et al. Detection of inflamed atherosclerotic lesions with diadenosine-5′,5′′′-P1,P4-tetraphosphate (Ap4A) and positron-emission tomography. Proc Nat Acad Sci U S A 2006;103: 15992–6.
14. Nahrendorf M, Zhang H, Hembrador S, et al. Nanoparticle PET-CT imaging of macrophages in inflammatory atherosclerosis. Circulation 2008;117: 379–87.
15. Rudd JH, Myers KS, Bansilal S, et al. Atherosclerosis inflammation imaging with ^{18}F-FDG PET: carotid, iliac, and femoral uptake reproducibility, quantification methods, and recommendations. J Nucl Med 2008;49: 871–8.
16. Rudd JH, Warburton EA, Fryer TD, et al. Imaging atherosclerotic plaque inflammation with [^{18}F]-fluorodeoxyglucose positron emission tomography. Circulation 2002;105:2708–11.
17. Tawakol A, Migrino RQ, Bashian GG, et al. In vivo ^{18}F-fluorodeoxyglucose positron emission tomography imaging provides a noninvasive measure of carotid plaque inflammation in patients. J Am Coll Cardiol 2006;48:1818–24.
18. Aziz K, Berger K, Claycombe K, Huang R, Patel R, Abela GS. Noninvasive detection and localization of vulnerable plaque and arterial thrombosis with computed tomography angiography/positron emission tomography. Circulation 2008;117:2061–70.
19. Calcagno C, Cornily JC, Hyafil F, et al. Detection of neovessels in atherosclerotic plaques of rabbits using dynamic contrast enhanced MRI and ^{18}F-FDG PET. Arterioscler Thromb Vasc Biol 2008;28:1311–7.
20. Poethko T, Schottelius M, Thumshirn G, et al. Two-step methodology for high-yield routine radiohalogenation of peptides: (18)F-labeled RGD and octreotide analogs. J Nucl Med 2004;45:892–902.
21. Allport JR, Lim YC, Shipley JM, et al. Neutrophils from MMP-9- or neutrophil elastase-deficient mice show no defect in transendothelial migration under flow in vitro. J Leuk Biol 2002;71: 821–8.
22. Nahrendorf M, Sosnovik D, Chen JW, et al. Activatable magnetic resonance imaging agent reports myeloperoxidase activity in healing infarcts and noninvasively detects the antiinflammatory effects of atorvastatin on ischemia-reperfusion injury. Circulation 2008;117:1153–60.
23. Shimizu K, Libby P, Shubiki R, et al. Leukocyte integrin Mac-1 promotes acute cardiac allograft rejection. Circulation 2008;117:1997–2008.
24. Hudson HM, Larkin RS. Accelerated image reconstruction using ordered subsets of projection data. IEEE transactions on medical imaging 1994; 13:601–9.
25. Weissleder R, Kelly K, Sun EY, Shtatland T, Josephson L. Cell-specific targeting of nanoparticles by multivalent attachment of small molecules. Nat Biotechnol 2005;23:1418–23.
26. Aikawa M, Sugiyama S, Hill CC, et al. Lipid lowering reduces oxidative stress and endothelial cell activation in rabbit atheroma. Circulation 2002;106: 1390–6.
27. Nahrendorf M, Swirski FK, Aikawa E, et al. The healing myocardium sequentially mobilizes two monocyte subsets with divergent and complementary functions. J Exp Med 2007;204: 3037–47.
28. Maekawa Y, Anzai T, Yoshikawa T, et al. Prognostic significance of peripheral monocytosis after reperfused acute myocardial infarction: a possible role for left ventricular remodeling. J Am Coll Cardiol 2002;39:241–6.
29. Mariani M, Fetiveau R, Rossetti E, et al. Significance of total and differential leucocyte count in patients with acute myocardial infarction treated with primary coronary angioplasty. Eur Heart J 2006;27: 2511–5.
30. Herskowitz A, Mayne AE, Willoughby SB, Kanter K, Ansari AA. Patterns of myocardial cell adhesion molecule expression in human endomyocardial biopsies after cardiac transplantation. Induced ICAM-1 and VCAM-1 related to implantation and rejection. Am J Pathol 1994;145: 1082–94.
31. Tanaka H, Sukhova GK, Swanson SJ, Cybulsky MI, Schoen FJ, Libby P. Endothelial and smooth muscle cells express leukocyte adhesion molecules heterogeneously during acute rejection of rabbit cardiac allografts. Am J Pathol 1994;144:938–51.
32. Hancock WW, Thomson NM, Atkins RC. Composition of interstitial cellular infiltrate identified by monoclonal antibodies in renal biopsies of rejecting human renal allografts. Transplantation 1983;35:458–63.
33. Kaufmann BA, Sanders JM, Davis C, Xie A, Aldred P, Sarembock IJ, Lindner JR. Molecular imaging of inflammation in atherosclerosis with targeted ultrasound detection of vascular cell adhesion molecule-1. Circulation 2007;116:276–84.

Key Words: atherosclerosis ■ inflammation ■ molecular imaging ■ PET-CT ■ VCAM-1.